Dynamical semigroup Fokker–Planck equation approach to transient absorption and fluorescence upconversion spectroscopies

Feng Shuang[a)]
Open Laboratory of Bond-Selective Chemistry, University of Science and Technology of China, Hefei, China and Department of Chemistry, Hong Kong University of Science and Technology, Kowloon, Hong Kong

Chen Yang and YiJing Yan[b)]
Department of Chemistry, Hong Kong University of Science and Technology, Kowloon, Hong Kong and Open Laboratory of Bond-Selective Chemistry, University of Science and Technology of China, Hefei, China

(Received 21 June 2000; accepted 6 December 2000)

A dynamical semigroup Fokker–Planck equation, which meanwhile satisfies also the semiclassical detailed-balance relation at arbitrary temperatures, is constructed and further applied to nonlinear spectroscopic processes of two-surface molecular systems in condensed phases. Included in dissipation are the T_1-vibrational relaxation and the pure T_2-dephasing in both nuclear and electronic degrees of freedom. A mixed Heisenberg–Schrödinger picture of the field-dressed optical response function is proposed to efficient evaluation of pulsed-laser spectroscopies. Numerical simulations are carried out in a model one-dimensional dissipative Morse molecular system. Both the pump–probe absorption and the time-frequency resolved fluorescence spectra are demonstrated and analyzed in detail in terms of the underlying dissipative dynamics. © *2001 American Institute of Physics.* [DOI: 10.1063/1.1344608]

I. INTRODUCTION

Time-resolved optical measurements using femtosecond or subpicosecond tunable laser pulses provide a versatile and real-time probe for molecular dynamics. However, the ability of extracting molecular information from spectroscopic measurements depends on a close interplay between theory and experiment. A molecular system in a condensed phase experiences not only energy relaxation but also decoherence (or dephasing), involved in both electronic and nuclear degrees of freedom. While the vibrational energy relaxation may be appropriately simulated with classical mechanics, pure-dephasing is of pure quantum in nature. Electronic dephasing, which is of fundamental importance especially to the interaction between the polar solute and polar solvent, has been understood spectroscopically as a result of a joint effort between theory and experiment in the past.[1–5] However, the pure vibrational dephasing remains largely unexplored. The electronic dephasing accounts largely for the effect of solvent dielectric fluctuation which modulates the chromophore's electronic energy band gap.[3–5] On the other hand, the pure vibrational dephasing accounts for the intraband (such as bandwidth and vibrational level structure) fluctuation that may due to the mechanical flexibility of large molecules in solutions. Vibrational coherence/decoherence plays an important role in some elementary photochemical and photobiological processes.[6–10] Furthermore, the understanding of vibrational dephasing will be crucial for recent activity in multidimensional off-resonant Raman spectroscopies.[11–21]

Quantum dissipation dynamics can be most conveniently described by the reduced system density operator $\rho(t)$. However, a quantum dissipation theory based on reduced description has to invoke certain approximation/model schemes for the statistical behaviors of system–bath coupling.[22] There are thus a variety of nonequivalent forms,[22] even within Markovian dissipation limit, of quantum dissipation theory, such as the Bloch–Redfield formulation,[23–27] a class of Fokker–Planck equations,[26–29] and the dynamical semigroup formulation.[30–32]

Moreover, the evaluation of nonlinear spectroscopies, which requires Liouville-space propagation in a two- or higher-dimensional time-grid, is numerically much more demanding than that of $\rho(t)$ itself or the linear spectroscopy. As a result, a Markovian formulation with a single equation of motion, rather than elaborated non-Markovian theories that consist usually of tens of coupled equations,[33–37] may be the practical choice to numerically study nonlinear spectroscopies.

In this work, we shall exploit a specific Markovian theory—Dynamical Semigroup Fokker–Planck Equation (DS-FPE)—for the numerically efficient evaluation of transient absorption and fluorescence signals. The optical medium is a two-surface molecular system involving vibrational T_1-relaxation and both electronic and nuclear pure T_2-dephasings. The DS-FPE to be presented is not only of the Lindblad's form,[30] but also of the detailed-balance up to the second-order cummulants in phase-space at arbitrary temperatures. The single-surface version of DS-FPE was developed recently,[27] together with its relations to other commonly used quantum dissipation formulations.[27]

The remainder of this paper is organized as follows: In

[a)]In partial fulfillment of the requirement for his Ph.D. degree at USTC.
[b)]Author to whom correspondence should be addressed. Electronic mail: yyan@ust.hk

Sec. II, we extend the previous one-surface formulation[27] to construct the DS-FPE for a two-surface dissipative molecular system under an optical excitation. The resulting DS-FPE is proved explicitly in Appendix A to be of the Lindblad's form.[30] In Sec. III, we examine how the DS-FPE can be used to efficiently evaluate the field-dressed optical response function, the key quantity in the interested nonlinear spectroscopies. The relation between the field-dressed response function and the conventional third-order nonlinear response functions[4] is analyzed in Appendix B. The transient absorption and fluorescence formulations are given in Sec. IV in terms of the field-dressed response function, while their derivations are detailed in Appendix C and Appendix D, respectively. In Sec. V, we present and discuss some numerical results of both the photoinduced molecular dynamics and nonlinear spectroscopies of a model dissipative molecular system. Finally, we summarize and conclude in Sec. VI.

II. A DYNAMICAL SEMIGROUP FOKKER–PLANCK EQUATION

Consider a molecular system embedded in a dissipative medium and interacting with a laser-pulse that resonantly couples two adiabatic molecular states, g and e. The dissipative dynamics assumes to be described by the Liouville equation (hereafter setting that $\hbar=1$),

$$\dot{\rho}(t)=-i[H(t),\rho(t)]-\mathcal{R}\rho(t). \tag{1}$$

Here, $\mathcal{R}$ is a dissipative superoperator that will be specified later in this section [cf. Eqs. (4)–(6)] to the completion of the dynamical semigroup Fokker–Planck equation (DS-FPE).

The reduced driven system Hamiltonian $H(t)$ in Eq. (1) assumes, under the electronic rotating-wave-approximation, the following form:[38]

$$H(t)=H_0-[D_+E(t)e^{-i\Delta\Omega t}+D_-E^*(t)e^{i\Delta\Omega t}]. \tag{2}$$

Here, $E(t)$ is the complex electric field envelop and $\Delta\Omega\equiv\Omega-\omega_{eg}$ the electronic detuning frequency of the excitation laser pulse, while

$$H_0=H_g|g\rangle\langle g|+H_e|e\rangle\langle e|, \tag{3a}$$

$$D_+=\mu|e\rangle\langle g|, \text{ and } D_-=\mu|g\rangle\langle e|. \tag{3b}$$

The molecular adiabatic Hamiltonian H_g or H_e, and the electronic dipole moment μ are operators in the nuclear subspace.

In this paper, we shall adopt a time-independent (Markovian) form for the dissipation superoperator $\mathcal{R}$ in Eq. (1). More precisely, we shall extend the previously constructed DS-FPE, i.e., Eqs. (48) and (49) with $\epsilon=0$ in Ref. 27, to the adiabatic two-surface molecular system considered here. The types of dissipation in consideration are the electronic pure T_2-dephasing, and the vibrational pure T_2-dephasing and vibrational T_1-relaxation in both adiabatic electronic states. Their rates are, respectively, specified as $\gamma_{\rm el}$, and (γ_2',γ_2'') and (γ_1',γ_1''). The parameter with a single-prime $'$ (double-prime $''$) is for the excited e (ground g) surface. The above individual dissipations are assumed to be statistically independent.

The final DS-FPE form of $\mathcal{R}$ in Eq. (1) assumes [cf. Eqs. (48) and (49) with $\epsilon=0$ in Ref. 27]

$$\mathcal{R}=\gamma_{\rm el}\mathcal{R}_{\rm el}+\gamma_2'\mathcal{R}_2'+\gamma_2''\mathcal{R}_2''+\gamma_1'\mathcal{R}_1'+\gamma_1''\mathcal{R}_1'', \tag{4}$$

with (denoting that $\hat{\mathbf{e}}\equiv|e\rangle\langle e|$ and $\hat{\mathbf{g}}\equiv|g\rangle\langle g|$),

$$\mathcal{R}_{\rm el}\rho=[\hat{\mathbf{e}},[\hat{\mathbf{e}},\rho]], \tag{5a}$$

$$\mathcal{R}_2'\rho=[H_e\hat{\mathbf{e}},[H_e\hat{\mathbf{e}},\rho]]/(\omega_0')^2, \tag{5b}$$

$$\mathcal{R}_1'\rho=-\frac{i}{4}[\{q-\overline{q'},p\}\hat{\mathbf{e}},\rho]+\frac{i}{2}[q\hat{\mathbf{e}},\{p\hat{\mathbf{e}},\rho\}] +\tfrac{1}{2}\overline{\sigma'}_{pp}[q\hat{\mathbf{e}},[q\hat{\mathbf{e}},\rho]]+\tfrac{1}{2}\overline{\sigma'}_{qq}[p\hat{\mathbf{e}},[p\hat{\mathbf{e}},\rho]]. \tag{5c}$$

$\mathcal{R}_2''$ and $\mathcal{R}_1''$ for the nuclear pure T_2-dephasing and T_1-relaxation on the ground electronic surface are defined similarly as Eqs. (5b) and (5c), respectively. In Eq. (5b), ω_0' is the harmonic frequency of the excited surface and is introduced to let $\mathcal{R}_2'$ be dimensionless. In Eq. (5c), $\{\cdot,\cdot\}$ denotes an anticommutator. Involved there are also three thermal equilibrium parameters,

$$\overline{q'}\equiv\langle q\rangle_e,\ \overline{\sigma'}_{qq}\equiv\langle(q-\overline{q'})^2\rangle_e, \text{ and } \overline{\sigma'}_{pp}\equiv\langle p^2\rangle_e. \tag{6}$$

Here $\langle A\rangle_n\equiv{\rm Tr}[\hat{A}\rho_{\rm eq}^{(n)}(T)]$, with $n=e$ or g, and

$$\rho_{\rm eq}^{(n)}(T)=\exp[-H_n/(k_BT)]/{\rm Tr}\exp[-H_n/(k_BT)], \tag{7}$$

being the equilibrium density operator on the specified surface. The detailed-balance requires $\rho_{\rm eq}^{(n)}(T)$ be a stationary solution to Eq. (1) in the absence of the external field.

Note that Eq. (5c) is written explicitly for molecular systems with a single vibrational degree of freedom. The extension to two-surface multidimensional molecular systems could be made in a straightforward manner, for example, by viewing q and p as vectors, while $\overline{\sigma}_{pp}$ and $\overline{\sigma}_{qq}$ as tensors.

Together with $\overline{p'}\equiv\overline{\sigma}'_{pq}=0$, the three parameters [Eq. (6)] involved explicitly in Eq. (5c) fully account for the first two moments of $\rho_{\rm eq}^{(e)}$. The above quantum dissipation formulation can be shown to have the exact detailed-balance relation for harmonic molecular systems.[27] In other words, the dissipation superoperator $\mathcal{R}$ presented in Eqs. (4)–(6) satisfies in general the detailed-balance property up to the second-order cummulants in the nuclear phase-space on each electronic surface at arbitrary temperatures.[27] Moreover, we shall in Appendix A show that each individual $\mathcal{R}$-contribution in Eq. (5) is of the Lindblad's dynamical semigroup form.[30] Equations (1)–(6) constitute the final DS-FPE formulation, and will be used in Sec. V for the numerical demonstrations of both the laser-induced dynamics and some nonlinear spectroscopies in a model anharmonic two-surface molecular system.

Each individual dissipation superoperator in Eq. (5) is defined in Schrödinger picture via its action-to-right, $\mathcal{R}\rho$, on the system density operator. For the later nonlinear spectroscopic calculation as well as theoretical completeness, we may also need its Heisenberg picture via the action-to-left, $\hat{A}\mathcal{R}$, on an arbitrary dynamical variable $\hat{A}$. It is easy to show that the Heisenberg counterparts of Eqs. (5a)–(5c) are

$$\hat{A}\mathcal{R}_{\rm el}=[[\hat{A},\hat{\mathbf{e}}],\hat{\mathbf{e}}], \tag{8a}$$

$$\hat{A}\mathcal{R}_2'=[[\hat{A},H_e\hat{\mathbf{e}}],H_e\hat{\mathbf{e}}]/(\omega_0')^2, \tag{8b}$$

$$\hat{A}\mathcal{R}_1'=-\frac{i}{4}[\hat{A},\{q-\overline{q}',p\}\hat{\mathbf{e}}]+\frac{i}{2}\{[\hat{A},q\hat{\mathbf{e}}],p\hat{\mathbf{e}}\} + \tfrac{1}{2}\sigma_{pp}'[[\hat{A},q\hat{\mathbf{e}}],q\hat{\mathbf{e}}]+\tfrac{1}{2}\sigma_{qq}'[[\hat{A},p\hat{\mathbf{e}}],p\hat{\mathbf{e}}]. \tag{8c}$$

The Heisenberg picture of $\mathcal{R}_2''$ and $\mathcal{R}_1''$ are defined similarly as Eq. (8b) and Eq. (8c), respectively.

III. FIELD-DRESSED RESPONSE FUNCTIONS

A. Green's function description

The optical response of $\rho(t)$, i.e., the dissipative and driven two-surface molecular system described by Eqs. (1)–(6), to a weak probe field can be expressed in terms of following field-dressed response function:

$$R_\pm(\tau,t)=i\,\mathrm{Tr}\{D_\mp\mathcal{G}(t+\tau,t)[D_\pm\rho(t)]\}. \tag{9}$$

Here, $D_\pm$ is the electronic transition dipole defined in Eq. (3b), and $\mathcal{G}$ is the Liouville-space Green's function or propagator for Eq. (1). That is, that $\mathcal{G}(t,t_0)\rho(t_0)\equiv\rho(t)$; with $t\geqslant t_0$. Note that the Hilbert-space version of $R_\pm$ in the absence of dissipation was given before.[39] The relation between $R_\pm$ and the conventional third-order nonlinear response functions[3,4] is presented in Appendix B.

Physically, $R_+(\tau,t)$ and $R_-(\tau,t)$ correspond to the absorptive and emissive responses, respectively, of the transient driven $\rho(t)$ interrogated locally by a weak probe field at t. They will be shown in the next section the key quantities in evaluating pump–probe absorption and time-frequency resolved fluorescence spectroscopies [cf. Eqs. (16)–(19)].

Obviously, $R_\pm$ [Eq. (9)] can be calculated step-by-step as follows:

$$\rho(t)\equiv\mathcal{G}(t,t_0)\rho(t_0), \tag{10a}$$

$$\rho_\pm(0;t)\equiv D_\pm\rho(t), \tag{10b}$$

$$\rho_\pm(\tau;t)\equiv\mathcal{G}(t+\tau,t)\rho_\pm(0,t), \tag{10c}$$

$$R_\pm(\tau,t)=i\,\mathrm{Tr}\{D_\mp\rho_\pm(\tau;t)\}. \tag{10d}$$

The above procedure may be said to implement $R_\pm$ [Eq. (9)] in Schrödinger picture, as each involving propagation is carried out by acting $\mathcal{G}$ on a state operator, $\rho(t_0)$ in Eq. (10a) or $\rho_\pm(0;t)$ in Eq. (10c). The Schrödinger picture of $R_\pm(\tau,t)$ [Eq. (10d)] requires the quantum propagation be carried out in a joint two-dimensional (τ,t)-grid, which is often numerically too demanding even for a one-dimensional dissipative molecular system.

B. A mixed Heisenberg–Schrödinger picture

In this subsection, we shall describe a mixed Heisenberg–Schrödinger picture of $R_\pm(\tau,t)$ [Eq. (9)] in which the (τ,t)-propagation can be largely disjointed, except for a small region during the pump excitation field interaction. In the context of pump–probe measurement, that is to say that the joint (τ,t)-propagation is needed only for the coherent spectroscopic contribution where the pump and the probe pulses overlap in time-domain.

As mentioned earlier, the t-argument in $R_\pm(\tau,t)$ denotes the moment at which the weak detection (probe) field interrogates with matter. For a sequential optical configuration in which the pump–probe field is ordered (i.e., first pump and then probe), the propagator $\mathcal{G}(t+\tau,t)$ in Eq. (9) reduces to the Green's function $\mathcal{G}_0(\tau)$ in the absence of time-dependent external driving field. We may therefore recast the sequential contribution to the field-dressed response function as[40,41]

$$R_\pm^S(\tau,t)\equiv i\,\mathrm{Tr}\{D_\mp\mathcal{G}_0(\tau)[D_\pm\rho(t)]\} \equiv i\,\mathrm{Tr}[D_\mp(\tau)D_\pm(0)\rho(t)]. \tag{11}$$

Here, the Heisenberg picture of $D_\pm$ or more general of an arbitrary dynamic variable $\hat{A}$ is defined as

$$\hat{A}(\tau)\equiv\hat{A}\mathcal{G}_0(\tau). \tag{12}$$

The corresponding Heisenberg equation of motion in the presence of dissipation is given by {cf. Eq. (1) with field-free H_0 [Eq. (3a)]}

$$\frac{\partial}{\partial\tau}\hat{A}=-i[\hat{A},H_0]-\hat{A}\mathcal{R}, \tag{13}$$

where $\hat{A}\mathcal{R}$ was given by Eqs. (4) and (8). The implementation of Eq. (11) involves therefore the propagations of $D_\mp(\tau)$ [Eq. (13)] and $\rho(t)$ [Eq. (1)] independently.

We are now in the position to propose a mixed Heisenberg–Schrödinger picture for the efficient numerical implementation of $R_\pm(\tau,t)$ [Eq. (9)] that accounts for both the sequential and coherent contributions. Let us denote the region of pump interaction as $[0,t_p]$. It is to say that the pump field $E(t>t_p)=0$ practically. Note that a propagator satisfies in general

$$\mathcal{G}(t+\tau,t)\equiv\mathcal{G}(t+\tau,t')\mathcal{G}(t',t);\ \text{with}\ t'\in[t+\tau,t]. \tag{14}$$

The above identity will be used whenever the breaking point can be chosen as $t'=t_p$. In this case, $\mathcal{G}(t+\tau,t'=t_p)=\mathcal{G}_0(t+\tau-t_p)$ the field-free Green's function, while $\mathcal{G}(t'=t_p,t)$ remains as the field-dressed propagator. The mixed Heisenberg–Schrödinger picture is then constructed by acting the field-free Green's function to its left onto the dynamic variable $D_\pm$ [cf. Eq. (12)], and the field-dressed part to its right onto the state variable $\rho_\pm(0,t)\equiv D_\pm\rho(t)$ [cf. Eq. (10c)].

The mixed Heisenberg–Schrödinger picture of $R_\pm(\tau,t)$ can be summarized as follows {cf. Fig. 1 with $[0,t_p]$ being the $E(t)$'s interaction region}:

Region I $(t\geqslant t_p)$ [cf. Eq. (11)]:

$$R_\pm(\tau,t)=R_\pm^S(\tau,t)=i\,\mathrm{Tr}[D_\mp(\tau)D_\pm\rho(t)]; \tag{15a}$$

Region II $(t+\tau\leqslant t_p)$ [cf. Eq. (10)]:

$$R_\pm(\tau,t)=i\,\mathrm{Tr}[D_\mp\rho_\pm(\tau,t)]; \tag{15b}$$

Region III $(\tau>t_p-t>0)$:

$$R_\pm(\tau,t)=i\,\mathrm{Tr}[D_\mp(t+\tau-t_p)\rho_\pm(t_p-t;t)]. \tag{15c}$$

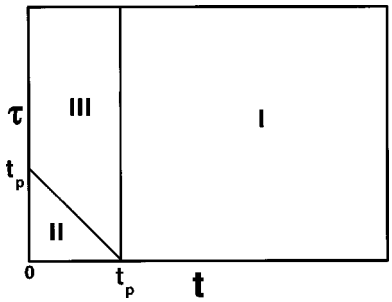

FIG. 1. Three regions for the calculation of field-dressed response function $R_{\pm}(\tau,t)$ in the mixed Heisenberg–Schrödinger picture [Eq. (15)]. t_p denotes the duration of the pump–matter interaction. The correlated (τ,t)-propagation is only needed in region II (see text).

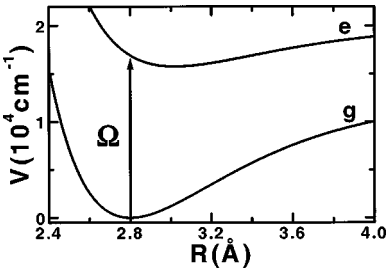

FIG. 2. Schematic diagram of the molecular system used in simulation. The potential parameters are given in Table I. The reduced molecular mass is $m=32$ amu. The central frequency of pump pulse is denoted as Ω. The molecule is initially in the thermal equilibrium in the ground electronic state manifold at $T=50$ K.

$R_{\pm}$ in Region I [Eq. (15a)] is the same as Eq. (11) and involves the disjoint τ-propagation and t-propagation. Only within the small triangle, Region II of Fig. 1, $R_{\pm}$ [Eq. (15b)] requires for the joint (t,τ)-propagation [Eq. (10)]. $R_{\pm}$ in Region III [Eq. (15c)] needs no extra propagation as it depends on the intermediate results from Eqs. (15a) and (15b). The mixed Heisenberg–Schrödinger picture of $R_{\pm}$ [Eq. (15)] will be used in Sec. V C for an efficient calculation of nonlinear spectroscopies.

IV. NONLINEAR SPECTROSCOPIES IN TERMS OF THE FIELD-DRESSED RESPONSE FUNCTION

In this section, we shall relate the field-dressed response function $R_{\pm}$ [Eq. (9) or (15)] to two types of nonlinear spectroscopies, pump–probe absorption and time-frequency resolved fluorescence. In both spectroscopic measurements, the detection fields assume to be operated in the weak response regime. The relevant optical polarizations that depend linearly on the detection field can be obtained via the standard first-order perturbation theory around the pump-driven dissipative system.

Let us start with the pump–probe absorption signals,[4,41–43] which can be recorded either as an integrated signal $S_A(t_d)$, or a frequency-dispersed transient absorption coefficient $\alpha(\omega,t_d)$. Here, t_d denotes the probe delay time with respect to the pump field. In Appendix C, we present the detailed derivation for $S_A(t_d)$ and $\alpha(\omega,t_d)$. Their final expressions are given in terms of the field-dressed response function $R_{\pm}$ [Eq. (9)] as

$$S_A(t_d) = -\mathrm{Im}\int_{-\infty}^{\infty} dt \int_0^{\infty} d\tau\, e^{i\Delta\Omega_T\tau} E_T^*(t+\tau)E_T(t) \times [R_+(\tau,t+t_d)+R_-^*(\tau,t+t_d)] \equiv S_+(t_d)+S_-(t_d), \tag{16}$$

$$\alpha(\omega,t_d) = -\mathrm{Im}\int_0^{\infty} d\tau\, e^{i\Delta\omega\tau}[R_+(\tau,t_d)+R_-^*(\tau,t_d)] \equiv \alpha_+(\omega,t_d)+\alpha_-(\omega,t_d). \tag{17}$$

In Eq. (16), $E_T(t)$ and $\Delta\Omega_T$ are the slowly varying complex envelop and the carrier detuning frequency of the probe field, respectively. In writing Eq. (17), we also assumed the impulsive probe approximation.[4] Defined in the second identities in Eq. (16) and Eq. (17) are also S_+ and $\alpha_{\pm}$. Physically, S_+ or α_+ (S_- or α_-) that arises from the R_+-term (R_--term) is the absorptive (emissive) contribution, monitoring the ground-surface ''hole'' (excite-surface ''particle'') wave packet dynamics.

We now turn to the time-frequency resolved fluorescence spectroscopies in which the spontaneous field should be treated as a quantum operator.[44] The fluorescence can be recorded either as the upconversion signal $S_E^{\mathrm{up}}(\omega,t_d)$ through a femtosecond-resolved sum frequency generation device,[45–48] or the scattered photon flux $S_E(\omega,t_d)$ with, for example, a CCD camera.[4,49] Here, t_d and ω denote the time and frequency centers of the detection gate. The fluorescence signals in the ideal time-frequency gate limit can be expressed as (cf. Appendix D for the derivation)

$$S_E^{\mathrm{up}}(\omega,t_d) = \left|\int_0^{\infty} d\tau\, e^{i\Delta\omega\tau} R_-^*(\tau,t_d-\tau)\right|^2, \tag{18}$$

$$S_E(\omega,t_d) = -\mathrm{Im}\int_0^{\infty} d\tau\, e^{i\Delta\omega\tau} R_-^*(\tau,t_d-\tau). \tag{19}$$

Note that the fluorescence signal S_E^{up} or S_E at time t_d [cf. Eqs. (18) or (19) together with Eq. (9)] depends on the reduced density operator $\rho(t_d-\tau)$ at all previous times (noting that $\tau\geqslant 0$). In contrast, the dispersed transient absorption α at t_d [cf. Eq. (17) with Eq. (9)] depends only on the local $\rho(t_d)$. The above temporal dependence in either fluorescence or transient absorption is consistent with the causality of the experimental configuration.

V. NUMERICAL RESULTS AND DISCUSSIONS

A. Simulation method and model

We shall present some calculation results on a model dissipative molecular system that will be specified soon. Demonstrated in Sec. V B will be the photoinduced dynamics of $\rho(t)$ [Eqs. (1)–(6)], while in Sec. V C the stationary absorption/emission, pump–probe absorption [Eqs. (16) and (17)], and time-frequency resolved fluorescence [Eqs. (18) and (19)] spectroscopies.

The molecule in study is modeled as a one-dimensional two-surface Morse system (cf. Fig. 2) with the reduced mass of $m=32$ amu. The potential parameters are given in Table I.

TABLE I. Parameters for the Morse potential surface, $V(R)=D_0[1-e^{-\alpha(R-R_0)}]^2$.

	$D_0/(\mathrm{cm}^{-1})$	$\alpha/(\text{Å}^{-1})$	$R_0/(\text{Å})$
V_g	12 550	1.871	2.80
V_e	4381	1.876	3.02

The resulting harmonic frequency of the ground electronic state is $\omega_0''=305.61\ \mathrm{cm}^{-1}$, while that of the excited surface is $\omega_0'=181.05\ \mathrm{cm}^{-1}$. The corresponding anharmonicity parameters are $\omega_0''\chi''=1.86\ \mathrm{cm}^{-1}$ and $\omega_0'\chi'=1.87\ \mathrm{cm}^{-1}$, respectively. The temperature is set to be $T=50$ K. The electronic transition dipole μ is set to be constant (Condon approximation). The dissipation parameters will be specified later.

The pump field is chosen as a 10 fs transform-limited Gaussian pulse with the excess carrier frequency of $\Delta\Omega=1143\ \mathrm{cm}^{-1}$. This frequency is near the peak of linear absorption spectroscopy (cf. Fig. 8). The intensity of the pump field is chosen such that $\mu E_{\mathrm{peak}}=300\ \mathrm{cm}^{-1}$, transferring about 15% of total population onto the excited potential surface when there are not any dissipations.

All calculations are carried out in the molecular vibrational eigenstate representation in the absence of an external driving field. The DVR method[50] is used to obtain the vibrational energies and wave functions. The number of vibrational states used in simulation (30 on the excited surface and 50 on the ground surface) is checked for numerical convergence. Quantum propagations to evaluate both $\rho(t)$ [Eqs. (1)–(6)] and $R_{\pm}(\tau,t)$ [Eq. (15) for its mixed Heisenberg–Schrödinger picture] are performed via the Short-Iterative-Arnoldi algorithm[25,51,52] with the cutoff out projection error of 10^{-7}.

We shall hereafter use the delay time t_d, with its time-zero centered at the peak of the given 10 fs transform-limit Gaussian pump field, to specify the dynamic time variable not only in the spectroscopic signals [Eqs. (16)–(19)] but also in the photoinduced $\rho(t_d)$.

B. Photoinduced molecular dissipative dynamics

This subsection will investigate the effect of vibrational T_1- and T_2-types of dissipation on $\rho(t_d)$ [Eqs. (1)–(6)] induced by the given resonant 10 fs pump laser pulse. The calculated ρ contains in general both the electronic populations, ρ_{ee} and ρ_{gg}, and the electronic coherence $\rho_{eg}=\rho_{ge}^{\dagger}$. To simplify the notation, we set $\gamma_1'=\gamma_1''=\gamma_1$ and $\gamma_2'=\gamma_2''=\gamma_2$, and remove single/double-prime(s) whenever it does not cause confusion. Although different values of dissipation could be chosen for the different electronic states, the general features of dissipation to be addressed would not be altered. After the 10 fs pump field is over, the pure electronic dephasing described in Eq. (5a) affects only ρ_{eg} in a rather simple manner, but plays no roles on ρ_{ee} or ρ_{gg}. For the clarity of demonstrating the effect of vibrational dissipations on the electronic coherence ρ_{eg} as well as the electronic populations, exemplified by ρ_{ee} in the following, the pure electronic dephasing parameter in this subsection is set to be $\gamma_{\mathrm{el}}=0$.

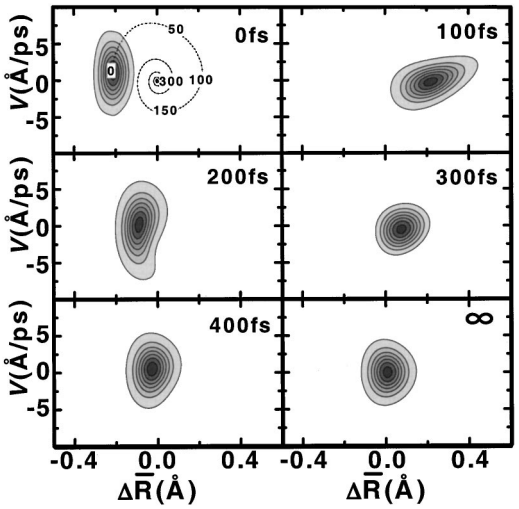

FIG. 3. The effect of vibrational T_1-relaxation on the photoexcited wave packet $\rho_{ee}(t_d)$ in the Wigner phase-space. The dissipation parameters are $\gamma_1=50\ \mathrm{cm}^{-1}$ and $\gamma_2=0$. The pump field is a 10 fs transform-limited Gaussian pulse with the excess-energy of $\Delta\Omega=1143\ \mathrm{cm}^{-1}$. The y-axis is presented in term of velocity. Indicated in each panel is the value of delay time t_d from where the pump pulse peaks. Included in the top-left panel is also the trajectory (dotted curve) of the phase-space center of ρ_{ee}.

1. Vibrational dissipations on the electronic populations

Let us start with the effect of vibrational T_1-relaxation on the electronic population, e.g., ρ_{ee}. Figure 3 depicts the evolution of $\rho_{ee}(\Delta R,p,t_d)$, with the dissipation parameters of $\gamma_1=50\ \mathrm{cm}^{-1}$ (i.e., $\gamma_1^{-1}=106$ fs) and $\gamma_2=0$, at the values of t_d specified in individual panels. Here, the coordinate-axis, $\Delta R=R-\overline{R'}$, denotes the diatomic bond displacement from the equilibrium length $\overline{R'}$ [cf. Eq. (6)] on the excited surface at the given temperature of $T=50$ K. The momentum-axis is given in terms of the velocity $v=p/m$ for ease of labeling unit. Included in the top-left panel is also the trajectory (dotted curve) of the nuclear phase-space center of $\rho_{ee}(t_d)$. The bottom-right panel presents the asymptotic $\rho_{ee}(t_d\to\infty)$, which is found to be practically identical to the exact thermal equilibrium density wave packet $\rho_{\mathrm{eq}}^{(e)}(T)$ in the electronic e state. The same quality of satisfying the detailed-balance relation is also found for $\rho_{gg}(t_d\to\infty)$ (not shown) in the electronic g state. Obviously, the wave packet $\rho_{ee}(t_d)$ remains pretty localized in phase-space.

We shall now turn to the effect of vibrational pure T_2-dephasing (γ_2) on the photoinduced ρ_{ee}. Figure 4 plots the $\rho_{ee}(t_d)$ with the dissipation parameters being set to be $\gamma_2=10\ \mathrm{cm}^{-1}$ and $\gamma_1=0$. In this case, there is no energy loss and the asymptotic $\rho_{ee}(t_d\to\infty)$ (the bottom-right panel) does not approach to the thermal equilibrium $\rho_{\mathrm{eq}}^{(e)}$. Included in the top-left panel is also an iso-energy loop (dotted curve) defined by the mean excess-energy of $\rho_{ee}(t_d)$ after the pump field is over. If the potential were harmonic, this isoenergy phase loop would be a circle (or an ellipse) and the pure vibrational dephasing dynamics could be solved analytically.[27] It is interesting that the pure dephasing may be mapped onto a classical heat transport problem with the pure-dephasing parameter γ_2 as the diffusion constant.[27] The

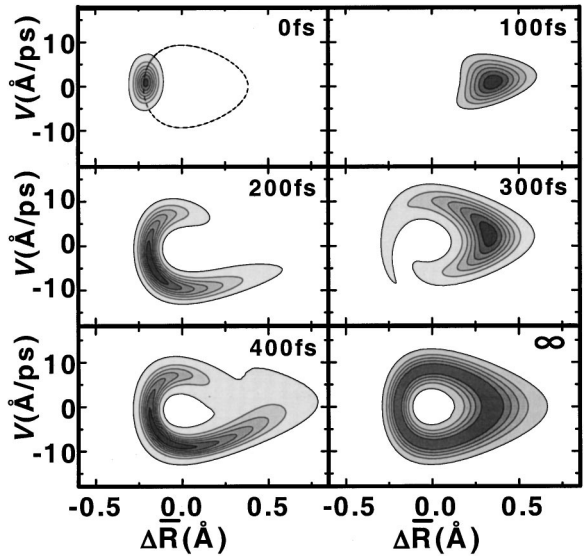

FIG. 4. Same as Fig. 3 but for the effect of vibrational pure T_2-dephasing. The dissipation parameters are $\gamma_1=0$ and $\gamma_2=10\ \mathrm{cm}^{-1}$. Included in the top-left panel is the isoenergy path (dotted curve) along which the vibrational pure-dephasing dynamics follows. See text for details.

basic features of vibrational pure dephasing that were obtained analytically before for a harmonic system[27] are now summarized for Fig. 4 in a semiquantitative manner as follows. (i) The coherent evolution of the phase-space center of $\rho_{ee}(t_d)$ travels clockwise around the isoenergy loop as indicated by the dotted curve in the top-left panel at the angular velocity defined by the classical frequency; (ii) The pure dephasing dynamics spreads $\rho_{ee}(t_d)$ over the isoenergy phase-loop at approximately the rate of γ_2.

Figures 5 and 6 depict the mean displacement $\Delta\bar{R}(t_d)\equiv\langle\Delta R(t_d)\rangle$ and the variance amplitude $\sigma_R(t_d)=(\langle R^2(t_d)\rangle-\langle R(t_d)\rangle^2)^{1/2}$, respectively, for the excited wave packet $\rho_{ee}(t_d)$ at the three indicated cases of dissipation. Note that in the harmonic limit, the Ehrenfest equations of motion for the first two moments of ρ_{ee} in phase-space, i.e., the Eq. (B1) of Ref. 27 with $\varepsilon=0$, can solved analytically. The resulting

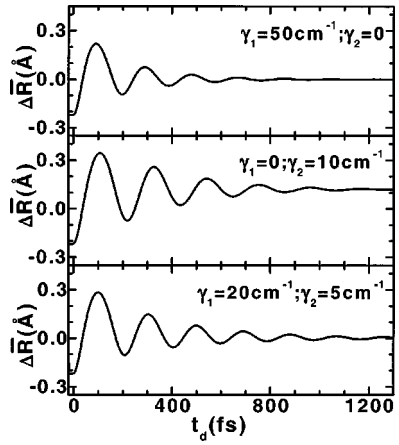

FIG. 5. Evolution of the mean displacement, $\Delta\bar{R}(t_d)\equiv\langle R(t_d)-\bar{R}'\rangle$, of $\rho_{ee}(t_d)$ in the presence of vibrational T_1-relaxation (top panel), or vibrational pure T_2-dephasing (middle panel), or both (bottom panel). The involving dissipation parameters are indicated in each panel.

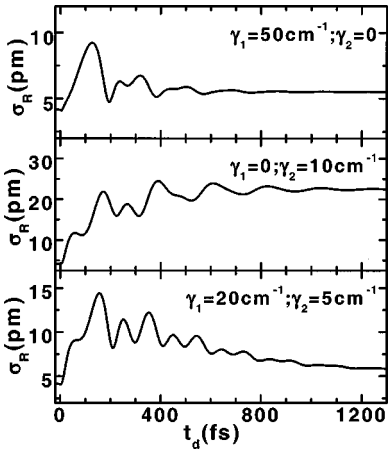

FIG. 6. Same as Fig. 5 but for the variance amplitude, $\sigma_R(t_d)=(\langle R^2(t_d)\rangle-\langle R(t_d)\rangle^2)^{1/2}$ of $\rho_{ee}(t_d)$.

$\langle R(t_d)\rangle$ and $\langle R^2(t_d)\rangle$ relax to their asymptotic values at the rates of $\gamma_1/2+\gamma_2$ and $\gamma_1+4\gamma_2$, respectively. When there is no pure dephasing, the wave packet remains pretty localized (cf. Fig. 3 and the top panel of Fig. 6). In this case, the peaks and valleys of $\Delta\bar{R}(t_d)$ (the top panel of Fig. 5) correspond to the classical outer and inner turning points, respectively, of the dissipative wave packet. In other words, the top panel of Fig. 5 is the coordinate representation of the classical trajectory shown in the dotted curve of the top-left panel of Fig. 3. However, in the case of vibrational pure T_2-dephasing, ρ_{ee} is neither localized nor a Gaussian-type wave packet (cf. Fig. 4). Therefore, one may not always be able to attribute the peaks/valleys of $\Delta\bar{R}(t_d)$, e.g., the middle panel of Fig. 5, to the classical turning points. It can be seen that the T_1-relaxation leads the quantum beats to be slightly up-chirped (cf. the top/bottom panel of Fig. 5) as the wave packet relaxes toward the bottom of the Morse potential well. The pure vibrational dephasing (cf. the middle panel of Fig. 5) that does not involve energy loss retains the simple mono-frequency quantum beats.

2. Vibrational dissipations on the electronic coherence

The vibrational T_1- or T_2-dissipation affects not only ρ_{ee} or ρ_{gg} but also the electronic coherence ρ_{eg} due to the Schwartz inequality.[53] It is unlike the pure electronic dephasing that leads to the decay of $\rho_{eg}=\rho_{ge}^{\dagger}\to 0$ but has no effect on the adiabatic dynamics of ρ_{ee} or ρ_{gg}. In order to show that the nuclear dissipation destroys also the molecular electronic phase, we introduce the electronic entropy as

$$s_{\mathrm{el}}(t_d)\equiv s(t_d)-s_{nu}(t_d), \tag{20}$$

with

$$s(t_d)=-\mathrm{Tr}[\rho(t_d)\ln\rho(t_d)], \tag{21a}$$

$$s_{nu}(t_d)=-\sum_{n=g,e}\mathrm{Tr}[\rho_{nn}(t_d)\ln\rho_{nn}(t_d)]. \tag{21b}$$

That $s_{\mathrm{el}}\to 0$ will be used in the following as an indicator of vanishing ρ_{eg}.

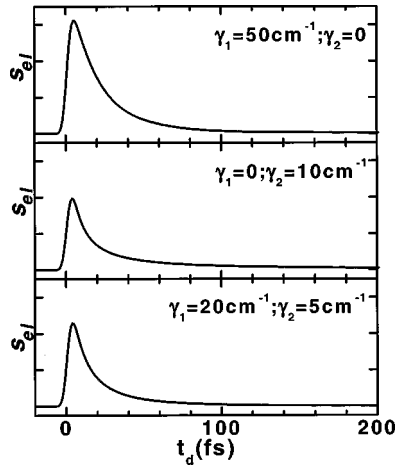

FIG. 7. Same as Fig. 5 but for the electronic entropy defined in Eq. (20) to demonstrate the effect of vibrational dissipation on the electronic dephasing of $\rho_{eg}=\rho_{ge}^{\dagger}$. The pure electronic dephasing parameter is set to be $\gamma_{\rm el}=0$.

Presented in Fig. 7 are the evolutions of electronic entropy $s_{\rm el}(t_d)$ in three specified cases of vibrational dissipation in the absence of pure electronic dissipation ($\gamma_{\rm el}=0$). The initial rise of electronic entropy $s_{\rm el}$ in Fig. 7 is due to the generation of electronic coherence $\rho_{eg}=\rho_{ge}^{\dagger}$ in the presence of the external 10 fs pump pulse field. Either the vibrational T_1-relaxation (top-panel), or the vibrational pure T_2-dephasing (middle-panel), or both (bottom-panel) can completely destroy the electronic coherence. Especially, a relatively small vibrational pure-dephasing γ_2 could resemble a significantly large effective electronic dephasing $\gamma_{el}^{\rm eff}$ (cf. the middle panel of Fig. 7). Moreover, the electronic dephasing induced via nuclear dissipation is *non-Markovian*, while that via a nonzero pure electronic $\gamma_{\rm el}$ is Markovian.

C. Spectroscopies

This subsection will present some numerical results of nonlinear absorption/fluorescence spectroscopies [Eqs. (16)–(19)] of the pulsed pump-driven molecular system with dissipation. The involving field-dressed response function $R_{\pm}$ will be implemented in its mixed Heisenberg–Schrödinger picture [Eq. (15)]. The vibrational dissipation parameters are chosen as $\gamma_1=\gamma_1'=\gamma_1''=20$ cm^{-1}, and $\gamma_2=\gamma_2'=\gamma_2''=5$ cm^{-1}. Included is also a pure electronic dephasing of $\gamma_{\rm el}=20$ cm^{-1}. Other parameters for the matter, the pump field, and the temperature were given in Sec. V A. The corresponding photoinduced molecular dynamics is described in Sec. V B (cf. the bottom panels of Figs. 5 and 6). The probe field will be specified when it is needed in due course.

1. Stationary absorption and emission

For the later discussion, we shall first present the stationary spectroscopies that relate to the following linear response functions:

$$J_{\pm}(\tau)=R_{\pm}^{S}(\tau,\mp\infty). \tag{22}$$

Here, $R_{\pm}^{S}$ is given in Eq. (11) with $D_{+}\rho(-\infty)=\mu\rho_{\rm eq}^{(g)}(T)$ and $D_{-}\rho(+\infty)=\mu\rho_{\rm eq}^{(e)}(T)$. That is, that $J_{+}(\tau)$ or $J_{-}(\tau)$ [Eq. (22)] is the optical response of the stationary density operator $\rho_{\rm eq}^{(n)}(T)$ [Eq. (7)] with $n=g$ or e, respectively. The conventional stationary absorption and fluorescence can be expressed in terms of the Fourier transform of $iJ_{+}(\tau)$ and $iJ_{-}^{*}(\tau)$, respectively.[4]

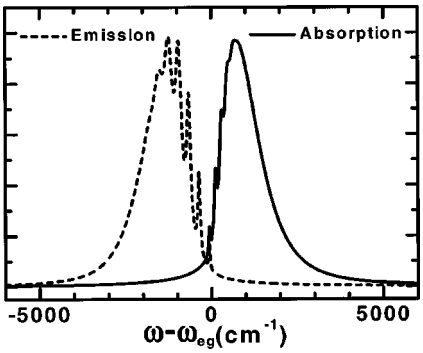

FIG. 8. Linear absorption (solid) and stationary fluorescence (dashed) spectroscopies at a temperature of 50 K. Dissipation parameters are $\gamma_1=20$ cm^{-1}, $\gamma_2=5$ cm^{-1}, and $\gamma_{\rm el}=20$ cm^{-1}.

Figure 8 depicts the stationary absorption (solid curve) and fluorescence (dashed curve) line shapes of the dissipative molecular system in study. These stationary spectroscopies will serve as asymptotic long-time results of the time-frequency resolved nonlinear optical signals to be presented later. Note that the stationary spectroscopies can be evaluated equally efficiently and accurately in either the Schrödinger or the Heisenberg pictures as discussed in Sec. III.

2. Transient pump–probe absorption signals

Figure 9 depicts the transient absorption signals $S_A(t_d)$ [Eq. (16), solid traces] detected at three values of probe detuning frequency $\Delta\Omega_T$ specified in individual panels. Each trace is presented the difference signal from its pump-off background. Included in each panel are also the absorptive S_{+} (dotted) and emissive S_{-} (dashed) contributions [cf. the second identity of Eq. (16)]. The probe field $E_T(t)$ is a 50 fs

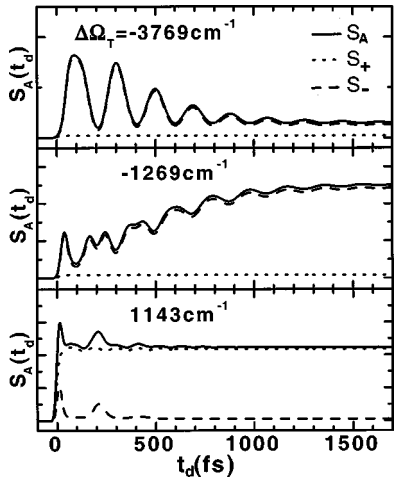

FIG. 9. Integrated transient absorption signals [Eq. (16)] at three representative detection frequencies indicated in individual panels (see the text for details). The observed signal $S_A(t_d)$ (solid) in each panel is a sum of two contributions: the absorptive contribution S_{+} (dotted) and the stimulated emission S_{-} (dashed). The dissipation bath is the same as that in Fig. 8.

transform-limited pulse. Physically, the three values of $\Delta\Omega_T$ in this figure are chosen to detect ρ_{ee} at the outer turning point region (top panel), an intermediate region (middle panel), and the inner turning point region (bottom panel), respectively, assuming there was no dissipation. To understand those seemingly very different spectroscopic patterns in the three panels, one should also refer to Fig. 8 for the relative positions of these three probe frequencies in the stationary absorption and emission spectra. Note the pump frequency with $\Delta\Omega = 1143\ \mathrm{cm}^{-1}$ is near the peak of linear absorption (cf. Fig. 8).

Let us start with the top panel of Fig. 9 in which the probe detuning $\Delta\Omega_T = -3769\ \mathrm{cm}^{-1}$ is at the outer turning point of the pump-induced ρ_{ee} before the dissipation taking place. The detection frequency is also near the red-wing of the stationary emission spectrum (cf. Fig. 8). The top panel exhibits therefore the following features. (i) The observed signal S_A is mainly from the stimulated emission component S_-, since the ground state ''hole'' described by $\rho_{gg} - \rho_{\mathrm{eq}}^{(g)}$ is away from the detection window; (ii) the quantum beats are singly peaked as the probe is placed to the outer turning point side; (iii) that the beats are slightly up-chirped is due to the vibrational T_1-relaxation of ρ_{ee} downward to the bottom of Morse potential well; (iv) the decay of quantum beats manifests the combinated effects of both the vibrational T_1-relaxation and the vibrational pure T_2-dephasing; and finally (v) the residual nonzero constant $S_A(t_d)$ at long t_d is attributed to the stationary emission stimulated by the probe field carrying the detuning frequency near the red-wing of the emission spectrum.

The seemingly very different signals in the middle and the bottom panels of Fig. 9 can also be understood similarly. The brief summary is as follows. Consider the spectral signal in the middle panel with $\Delta\Omega_T = -1269\ \mathrm{cm}^{-1}$. Here, the first few doubly-split peaks are due to the probe frequency being in between of two turning points, resulting in a double crossing of the wave packet over the detection region in each period. As time evolves, the wave packet relaxes into the detection region where the stationary emission is relatively strong (cf. Fig. 8). As results, the doubly-split peaks merge into singly-peaked beats and the stimulated emission becomes stronger as it approaches to the stationary background intensity. In contrast, the signal background strength in the bottom panel of Fig. 9 arises mainly from the ground state ''hole'' contribution S_+, since the detection detuning $\Delta\Omega_T = 1143\ \mathrm{cm}^{-1}$ is the same as that of pump and locates near the stationary absorption maximum (cf. Fig. 8). The evolution of the initially excited ''particle'' wave packet ρ_{ee} can only be observed within a few periods before it relaxes away from the probe window. However, the ground state ''hole'' wave packet $\rho_{gg} - \rho_{\mathrm{eq}}^{(g)}$ remains within the resonant absorptive detection region, leading to the large absorptive background strength in the bottom panel of Fig. 9.

3. Time-frequency resolved absorption spectroscopies

Figure 10 presents the calculated time-frequency resolved signal $\alpha(\omega, t_d)$ [Eq. (17)], also in the form of difference signal, with the removal of the pump-off stationary background or the stationary absorption in Fig. 8. It can be seen that in the short-t_d regime, the absorptive and emissive components, α_+ and α_- [cf. the second identity of Eq. (17)], overlap in the frequency-domain. As the time t_d evolves, the absorptive component α_+ remains in about the same frequency region, while the stimulated emission component α_- experiences dynamic Stokes shift. In the long-t_d regime, the α_+ and the α_- components are shown to coincide respectively with the stationary absorption and the stationary emission as indicated in Fig. 8.

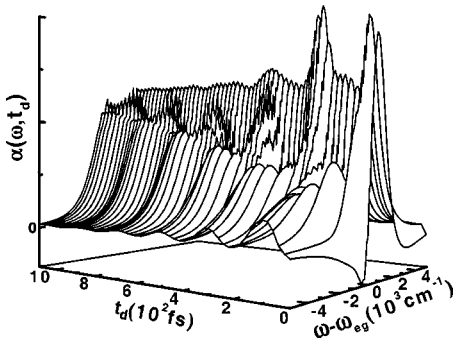

FIG. 10. Dispersed transient absorption coefficient, $\alpha(\omega, t_d)$ [Eq. (17)]. The dissipation bath is the same as that in Fig. 8.

It is well known that the pump–probe transient absorption, either the integrated signal $S_A(t_d)$ [Eq. (16)] or the dispersed signal $\alpha(\omega, t_d)$ [Eq. (17)], can be formally considered as a sum of the sequential and the coherent contributions.[4,42] Let us use the dispersed absorption coefficient for illustration, $\alpha(\omega, t_d) \equiv \alpha^S(\omega, t_d) + \alpha^C(\omega, t_d)$. The sequential contribution assumes the same form of Eq. (17), i.e., $\alpha^S = \alpha_+^S + \alpha_-^S$, but with the field-dressed response function $R_\pm$ in Eq. (17) being replaced by its sequential counterpart $R_\pm^S$ [Eq. (11)]. Once α (or $\alpha_\pm$) and α^S (or $\alpha_\pm^S$) are evaluated, the coherent contribution α^C (or $\alpha_\pm^C$) is obtained as their difference. Obviously, for the well-separated pump–probe configuration, the sequential part $\alpha^S(\omega, t_d)$ is the sole signal contribution [cf. Eq. (15a) together with its applicable region]. However, when pump and probe overlap in time, the coherent part $\alpha^C(\omega, t_d)$ may constitute an important contribution to the observed signal $\alpha(\omega, t_d)$.

The top panel of Fig. 11 depicts the observed $\alpha(\omega, t_d = 0)$ (solid) as the sum of α^S (dotted) and α^C (dashed) at $t_d = 0$, at which the pump and the probe overlap maximally. Obviously, the coherent contribution α^C can be of the same order as or larger than the sequential contribution α^S when the pulses overlap. The middle (bottom) panel of Fig. 11 analyzes α^C (α^S) further in terms of its absorptive α_+^C (α_+^S) and stimulated emission α_-^C (α_-^S) components. Note that the coherent contribution (the middle panel of Fig. 11) has some significant negative values in some frequency region, especially in its absorptive component α_+^C. In fact, the concept of being absorptive/emissive may only be physically correct for the sequential $\alpha_\pm^S$ contribution (the bottom panel of Fig. 11). According to the Eq. (B3), α_+^C involves three Liouville-space (R_1, R_4, and R_2) pathways and α_-^C only the R_3 pathway in the conventional weak response third-order response function formalism.[3,4] This may account for why, as shown

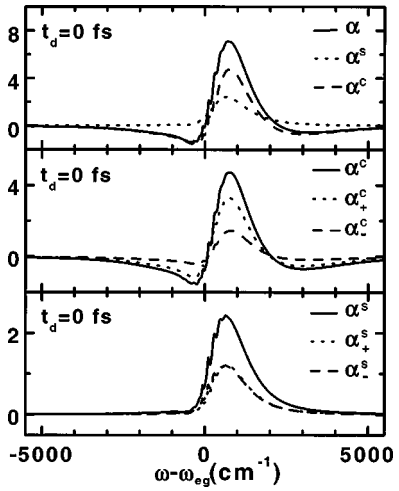

FIG. 11. (Top panel) Dispersed transient signal α (solid) at the $t_d=0$ slice analyzed in terms of its coherent α^C (dashed) and sequential α^S (dotted) contributions; (middle panel) α^C (solid) is further analyzed in terms of its two components, α^C_+ (dotted) and α^C_- (dashed); (bottom panel) α^S (solid) is further analyzed in terms of its two components, α^S_+ (dotted) and α^S_- (dashed).

in the middle panel of Fig. 11, the magnitude of α^C_+ is larger than that of α^C_-. Equation (B3) implies also that α^C_+ may be more properly called as the excitation Raman contribution, while α^C_- is the stimulated emission Raman contribution. The negative values in $\alpha^C_\pm$ (cf. the top panel of Fig. 11) thus indicate the underlying coherent Raman processes.[4]

4. Time-frequency resolved fluorescence signals

Let us now consider the time-frequency resolved fluorescence signals. Figure 12 plots the spontaneous emission $S_E(\omega,t_d)$ [Eq. (19), solid curves], fluorescence upconversion $S^{\rm up}_E$ [Eq. (18), dotted curves], together with the stimulated emission $\alpha_-(\omega,t_d)$ (dashed curves) at some representing values of t_d as specified in individual panels. $S^{\rm up}_E$ [Eq. (18)] and $S_E(\omega,t_d)$ [Eq. (19)] contain basically the same dynamic information, and their difference is mainly due to the amplitude square in relation with the amplitude itself. The spontaneous emission S_E (solid curves) and the stimulated emission α_- (dashed curves) are only different in the short time regime (two top panels), but evolve to be identical (two bottom panels) as the results of dissipation that suppresses the memory effect. At the long time regime (cf. bottom right panel) both S_E and α_- coincide with the stationary emission spectrum, i.e., the dashed curve in Fig. 8.

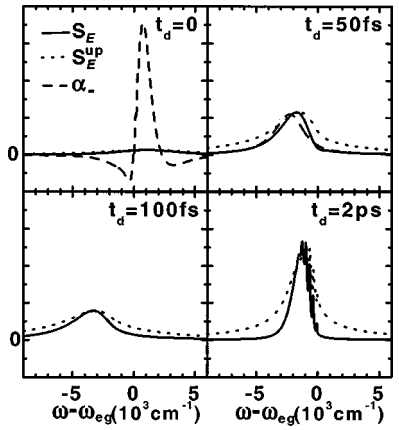

FIG. 12. Comparison among the ordinary fluorescence S_E [solid, Eq. (17)], fluorescence upconversion $S^{\rm up}_E$ [dotted, Eq. (18)], and the stimulated emission α_- [dashed, cf. Eq. (17)] at four representing delay times.

VI. SUMMARY AND CONCLUDING REMARKS

In summary, we have constructed a dynamical semigroup Fokker–Planck equation (DS-FPE) and further implement it to nonlinear optical processes involving two-surface molecular systems in condensed phases. The obtained DS-FPE (Sec. II), which can be considered as the natural extension of the counterpart in one-surface molecular systems,[27] is given in both Schrödinger and Heisenberg pictures. We also proposed a mixed Heisenberg–Schrödinger prescription of the field-dressed optical response function (Sec. III) for the efficient calculation of nonlinear spectroscopies presented in Sec. V.

Numerical demonstrations are made for both the photoinduced molecular dissipative dynamics $\rho(t)$ (Sec. V B) and various spectroscopies (Sec. V C). Highlighted in the photoinduced molecular dynamics are the effects of vibrational T_1- and T_2-types of dissipation on the electronic coherence ρ_{eg} as well as on the electronic population ρ_{ee} or ρ_{gg}. Included in the spectroscopic calculations are the stationary absorption and fluorescence, the integrated and the dispersed transient absorption, and the time-frequency resolved fluorescence spectroscopies in the presence of the aforementioned vibrational dissipation and the pure electronic dephasing. Detailed comparisons among various spectroscopies are made in conjunction with the underlying dissipative molecular dynamics.

Presented in Sec. IV are the pump–probe absorption and the time-frequency resolved fluorescence formulations in terms of field-dressed response function. Their polarization counterparts are given in Appendices C and D, respectively. Both the response-function formalism and the polarization formalism of nonlinear spectroscopies outlined in this work can be readily implemented via other forms of Markovian[23–32] or non-Markovian[33–37] quantum dissipation theory.

Considered explicitly in this work is only a single optically active mode (vibration) that couples to the optical transition. This active mode experiences both T_1-relaxation and pure T_2-dephasing and is taken to be in the underdamped regime. We have demonstrated that the Markovian vibrational T_1- or/and T_2-dissipation(s) can introduce an effective non-Markovian electronic dephasing (cf. Fig. 7 and its discussion). The resulting vibrational relaxation-induced dynamic Stokes-shift is evident (cf. Figs. 10 and 12). The inclusion of multiple dissipative modes, especially of an overdamped solvation mode to account for bath reorganization-induced Stokes-shift,[3,4,41] can be done and will be published in the future.

ACKNOWLEDGMENTS

The support of the Research Grants Council of Hong Kong Government and the National Natural Science Foundation of China is gratefully acknowledged.

APPENDIX A: DYNAMICAL SEMIGROUP DISSIPATION

Lindblad showed that a Markovian quantum dissipation theory satisfying the general positivity should be of the following form of dissipation:[30]

$$\mathcal{R}\rho=\sum_{\alpha}\,[W_{\alpha}^{\dagger},W_{\alpha}\rho]+\text{H.c.} \tag{A1}$$

Obviously, $\mathcal{R}_{\rm el}$ [Eq. (5a)] and $\mathcal{R}_2'$ [Eq. (5b)] are of the Lindblad's form. In the following, we shall use the similar algorithm in our previous work[27] to show that $\mathcal{R}_1'$ [Eq. (5c)] can also be transformed into the Lindblad's form.

To proceed, let us denote

$$\hat{W}\equiv\frac{(q-\overline{q'})\hat{\mathbf{e}}}{\sqrt{4\overline{\sigma'_{qq}}}}+i\frac{p\hat{\mathbf{e}}}{\sqrt{4\overline{\sigma'_{pp}}}}. \tag{A2}$$

We have

$$(q-\overline{q'})\hat{\mathbf{e}}=\sqrt{\overline{\sigma'_{qq}}}(\hat{W}+\hat{W}^{\dagger}), \tag{A3a}$$

$$p\hat{\mathbf{e}}=-i\sqrt{\overline{\sigma'_{pp}}}(\hat{W}-\hat{W}^{\dagger}), \tag{A3b}$$

We shall also denote ($\hbar\equiv1$),

$$\eta\equiv\sqrt{4\overline{\sigma'_{pp}}\overline{\sigma'_{qq}}}\geqslant1. \tag{A4}$$

The inequality is the uncertainty relation.

Equation (5c) can now be recast as

$$\mathcal{R}_1'\rho=\frac{\eta}{2}\cdot I+\frac{\eta^2}{4}\cdot\text{II}, \tag{A5}$$

where

$$\begin{aligned}\text{I}&\equiv-\tfrac{1}{4}[\{\hat{W}+\hat{W}^{\dagger},\hat{W}-\hat{W}^{\dagger}\},\rho]+\tfrac{1}{2}[\hat{W}+\hat{W}^{\dagger},\{\hat{W}-\hat{W}^{\dagger},\rho\}]\\&=\tfrac{1}{2}[\hat{W}^{\dagger},\hat{W}\rho]-\tfrac{1}{2}[\hat{W},\hat{W}^{\dagger}\rho]+\text{H.c.}\end{aligned} \tag{A6a}$$

$$\begin{aligned}\text{II}&\equiv\tfrac{1}{2}[\hat{W}+\hat{W}^{\dagger},[\hat{W}+\hat{W}^{\dagger},\rho]]-\tfrac{1}{2}[\hat{W}-\hat{W}^{\dagger},[\hat{W}-\hat{W}^{\dagger},\rho]\\&=[\hat{W}^{\dagger},\hat{W}\rho]+[\hat{W},\hat{W}^{\dagger}\rho]+\text{H.c.}\end{aligned} \tag{A6b}$$

We have therefore [cf. Eq. (A5)]

$$\mathcal{R}_1'\rho=\eta_{+}[\hat{W}^{\dagger},\hat{W}\rho]+\eta_{-}[\hat{W},\hat{W}^{\dagger}\rho]+\text{H.c.}, \tag{A7}$$

with $\eta_{\pm}\equiv\frac{1}{4}\eta(\eta\pm1)\geqslant0$ [cf. Eq. (A4)]. Therefore, $\mathcal{R}_1'\rho$ in Eq. (A7) consists of two Lindblad's terms [cf. Eq. (A1)] and is of general positivity. We have thus completed the proof that the quantum Fokker–Planck formulation, Eqs. (1)–(6), is of the general positivity. Q.E.D.

APPENDIX B: RELATION TO THE THIRD-ORDER NONLINEAR RESPONSE FUNCTIONS

In this appendix, we shall expand the field-dressed response function $R_{\pm}(\tau,t)$ [Eq. (9)] in the second-order of pump excitation field E, and thus establish its relation to the conventional material third-order nonlinear response function formulations in the weak field regime.[4] Note that as it describes the response of pump-driven system to the first order in probe field, $R_{\pm}$ in its nth-order pump-field expansion form relates in general with the conventional $(n+1)$th-order material nonlinear response functions.

Before proceeding, we first notice that in $R_{\pm}(\tau,t)$ the action of probe field occurs at time t. Therefore, we may decompose the field-dressed response function into the sequential and the coherent contributions,[4,41]

$$R_{\pm}(\tau,t)\equiv R_{\pm}^{S}(\tau,t)+R_{\pm}^{C}(\tau,t). \tag{B1}$$

The sequential contribution $R_{\pm}^{S}$ is given by Eq. (11) and describes the process in which the action of (probe) detection field takes place after that of pump. Once the sequential contribution is determined, the coherent contribution can be obtained via Eq. (B1), or $R_{\pm}^{C}\equiv R_{\pm}-R_{\pm}^{S}$. Obviously, the coherent response contributes only when the pump and the probe overlap, while the sequential response $R_S(\tau,t)$ contributes when the pulses overlap as well as they are separated.

In the weak field limit, we can expand both the sequential and coherent contributions to the second order in the excitation field, resulting in

$$\begin{aligned}R_{+}^{S}(\tau,t)=(i/\hbar)^3\int_0^{\infty}dt_2\int_0^{\infty}dt_1\,[&e^{i\Delta\Omega t_1}E^{*}(t-t_2)\\&\times E(t-t_2-t_1)R_4(\tau,t_2,t_1)+e^{-i\Delta\Omega t_1}\\&\times E(t-t_2)E^{*}(t-t_2-t_1)R_3(\tau,t_2,t_1)],\end{aligned} \tag{B2a}$$

$$\begin{aligned}[R_{-}^{S}(\tau,t)]^{*}=(i/\hbar)^3\int_0^{\infty}dt_2\int_0^{\infty}dt_1\,[&e^{i\Delta\Omega t_1}E^{*}(t-t_2)\\&\times E(t-t_2-t_1)R_1(\tau,t_2,t_1)+e^{-i\Delta\Omega t_1}\\&\times E(t-t_2)E^{*}(t-t_2-t_1)R_2(\tau,t_2,t_1)],\end{aligned} \tag{B2b}$$

and

$$\begin{aligned}R_{+}^{C}(\tau,t)=(i/\hbar)^3\int_0^{\infty}dt_3\int_0^{\infty}dt_2\,&e^{-i\Delta\Omega t_2}E(t+\tau-t_3)\\&\times E^{*}(t+\tau-t_2-t_3)[R_1(t_3,t_2,\tau-t_2-t_3)\\&+R_4(t_3,t_2,\tau-t_2-t_3)]+(i/\hbar)^3\\&\times\int_0^{\infty}dt_2\int_0^{\infty}dt_1\,e^{-i\Delta\Omega(t_1+t_2)}E(t+t_2)\\&\times E^{*}(t-t_1)R_2(\tau-t_2,t_2,t_1),\end{aligned} \tag{B3a}$$

$$\begin{aligned}[R_{-}^{C}(\tau,t)]^{*}=(i/\hbar)^3\int_0^{\infty}dt_2\int_0^{\infty}dt_1\,&e^{-i\Delta\Omega(t_1+t_2)}\\&\times E(t+t_2)E^{*}(t-t_1)R_3(\tau-t_2,t_2,t_1).\end{aligned} \tag{B3b}$$

Here, $R_{\alpha}(t_3,t_2,t_1)$; $\alpha=1,...,4$, are the four well-known third-order nonlinear response functions for two surfaces molecular systems.[4] The conventional third-order response function formulations of the pump–probe absorption[4,41,42] can then be recovered via the above equations together with Eq. (16) or (17), the that of time-frequency resolved fluorescence[4,47–49] with Eqs. (18) or (19), respectively.

APPENDIX C: PUMP–PROBE ABSORPTION: DERIVATION OF EQS. (16) AND (17)

Let us start with the standard optical polarization formulation for pump–probe absorption spectroscopies,[4,41]

$$S_A(t_d) = -\,\mathrm{Im}\int_{-\infty}^{\infty} dt\, E_T^*(t-t_d) P_{\mathbf{k}_T}(t;t_d), \tag{C1}$$

$$\alpha(\omega,t_d) = -\,\mathrm{Im}[\tilde{P}_{\mathbf{k}_T}(\omega,t_d)/\tilde{E}_T(\omega)]. \tag{C2}$$

Here, $P_{\mathbf{k}_T}(t;t_d)$ is the optical polarization at the detection direction $\mathbf{k_T}$, while

$$\tilde{P}_{\mathbf{k}_T}(\omega;t_d) \equiv \int_{-\infty}^{\infty} dt\, e^{i(\omega-\Omega_T)(t-t_d)} P_{\mathbf{k}_T}(t;t_d), \tag{C3}$$

and $\tilde{E}_T(\omega)$ is defined similarly. The time argument in the probe field $E_T(t-t_d)$ accounts for its center being t_d-delayed from that of the pump field $E(t)$.

The key quantity here is the complex polarization function, $P_{\mathbf{k}_T}(t;t_d)$, which in the weak probe regime, depends linearly on the probe detection field E_T at the $\mathbf{k}_T$-direction but not on the complex conjugate part E_T^* at the opposite direction.[4] In other words, we shall consider the standard first-order perturbation theory with respect to the following system-probe interaction in RWA:

$$\delta H_{\mathbf{k}_T}(t) = -D_+ E_T(t-t_d) e^{-i\Delta\Omega_T(t-t_d)}. \tag{C4}$$

The corresponding first-order density operator $\delta\rho_{\mathbf{k}_T}(t;t_d)$ can then be obtain via [cf. Eq. (1)]

$$\delta\dot{\rho}_{\mathbf{k}_T}(t;t_d) = \mathcal{L}_{\mathrm{FP}}(t)\,\delta\rho_{\mathbf{k}_T}(t;t_d)] + iE_T(t-t_d)e^{-i\Delta\Omega_T(t-t_d)}[D_+,\rho(t)], \tag{C5}$$

with the initial condition $\delta\rho_{\mathbf{k}_T}(-\infty;t_d)=0$, and [cf. Eq. (1)]

$$\mathcal{L}_{\mathrm{FP}}(t) \equiv -i[H(t),\ldots] - \mathcal{R}. \tag{C6}$$

The polarization function can then be evaluated as

$$P_{\mathbf{k}_T}(t;t_d) = e^{i\Delta\Omega_T(t-t_d)}\,\mathrm{Tr}[D_-\,\delta\rho_{\mathbf{k}_T}(t;t_d)]. \tag{C7}$$

The above equations constitute the polarization formalism of pump–probe absorption spectroscopies.[34,43]

To derive the field-dressed response function formalism, Eqs. (16) and (17), we shall formally integrate Eq. (C5), resulting in

$$\delta\rho_{\mathbf{k}_T}(t;t_d) = i\int_{-\infty}^{t} d\tau\, e^{-i\Delta\Omega_T(\tau-t_d)} E_T(\tau-t_d) \times \mathcal{G}(t,\tau)[D_+\rho(\tau) - \rho(\tau)D_+]. \tag{C8}$$

By using the above equation, together with the identity, $\mathrm{Tr}\{D_-\mathcal{G}(t,\tau)[\rho(\tau)D_+]\} = \mathrm{Tr}\{D_+\mathcal{G}(t,\tau)[D_-\rho(\tau)]\}^*$, followed by changing the integration variable from $t-\tau$ to τ, we can recast Eq. (C7) as

$$P_{\mathbf{k}_T}(t;t_d) = \int_0^{\infty} d\tau\, e^{i\Delta\Omega_T\tau} E_T(t-\tau-t_d) \times [R_+(\tau,t-\tau) + R_-^*(\tau,t-\tau)]. \tag{C9}$$

Here, $R_\pm$ was given by Eq. (9). Equation (16) can then be obtained by substituting Eq. (C9) into Eq. (C1), followed by a proper change of integration variables.

For an impulsive probe field, the field-dress function $R_\pm(\tau,t-\tau)$ in Eq. (C9) can be replaced by $R_\pm(\tau,t_d)$. The resulting $P_{\mathbf{k}_T}(t;t_d)$ is transformed into $\tilde{P}_{\mathbf{k}_T}(\omega,t_d)$ [Eq. (C3)], and then used in Eq. (C2), resulting in Eq. (17). Q.E.D.

APPENDIX D: SPONTANEOUS EMISSION: DERIVATION OF EQS. (18) AND (19)

Spontaneous emission is nondirectional. Its polarization may however be defined similarly as Eq. (C7) but with the inclusion of the quantum field creation and annihilation operators, $\hat{a}_S^\dagger$ and $\hat{a}_S$. In connection with Eq. (C4), let us cast the quantum field-matter interaction as[4,44]

$$\delta H_S(t) = -i\varepsilon_S D_+ \hat{a}_S e^{-i\Delta\omega_S t} + H.c. \tag{D1}$$

Here, $\varepsilon_S \equiv e[\hbar\omega_S/(2\epsilon_0 V)]^{1/2}$, with e being the electron charge, ϵ_0 the electric permittivity of free space, and V the quantization volume. The spontaneous emission polarization may then be given as [cf. Eq. (C7)]

$$P_{\omega_S}(t) = -ie^{i\Delta\omega_S t}\,\hat{\mathrm{Tr}}[D_-\hat{a}_S^\dagger\delta\hat{\rho}(t;\Delta\omega_S)]. \tag{D2}$$

The trace, $\hat{\mathrm{Tr}} \equiv \mathrm{Tr}\cdot\mathrm{Tr}_S$, runs over both the molecular and the quantum field subspaces. The spontaneous emission field is initially in the vacuum state, $\rho_S(-\infty) = |0_S\rangle\langle 0_S|$, satisfying $[a_S,\rho_S(-\infty)] = -|0_S\rangle\langle 1_S|$. Thus, $\delta\hat{\rho}$ in Eq. (D2) assumes the form [cf. Eq. (C8)]

$$\delta\hat{\rho}(t;\Delta\omega_S) = \delta\rho(t;\Delta\omega_S)|0_S\rangle\langle 1_S|, \tag{D3}$$

where

$$\delta\rho(t;\Delta\omega_S) = \varepsilon_S\int_{-\infty}^{t} d\tau\, e^{-i\Delta\omega_S\tau}\mathcal{G}(t,\tau)[\rho(\tau)D_+]. \tag{D4}$$

Substituting Eq. (D3) into Eq. (D2), followed by tracing over the quantum field subspace, we obtain [cf. Eq. (C9)]

$$P_{\omega_S}(t) = -ie^{i\Delta\omega_S t}\,\mathrm{Tr}[D_-\,\delta\rho(t;\Delta\omega_S)] = \varepsilon_S\int_0^{\infty} d\tau\, e^{i\Delta\omega_S\tau} R_-^*(\tau,t-\tau). \tag{D5}$$

Note that from Eq. (D4), we have [cf. Eq. (C5)]

$$\delta\dot{\rho}(t;\Delta\omega_S) = \mathcal{L}_{\mathrm{FP}}\delta\rho(t;\Delta\omega_S) + \varepsilon_S e^{-i\Delta\omega_S t}\rho(t)D_+. \tag{D6}$$

The upconversion detection scheme introduces effectively a time-frequency window function $w(\omega_S,t)$, assumed to be centered at ω and t_d, to gate the dispersed transient fluorescence.[45–48] The resulting upconversion signal can thus be expressed as $S_E^{\mathrm{up}}(\omega,t_d) = |w(\omega-\omega_S,t-t_d)\otimes P_{\omega_S}(t)|^2$. Here, $\otimes$ denotes the time-frequency double integration. On the other hand, the ordinary fluorescence signal detected, for example with a CCD camera, as the scattered photon flux can be expressed as $S_E(\omega_S;t) = -\,\mathrm{Im}\,P_{\omega_S}(t)$, convoluted with a real time-frequency gate function.

In the ideal case in which the time-frequency gate can be considered as a delta function in both time and frequency domains, we have

$$S_E^{\mathrm{up}}(\omega,t_d)=|P_\omega(t_d)|^2\,, \tag{D7}$$

$$S_E=-\operatorname{Im}P_\omega(t_d)\,. \tag{D8}$$

Equations (18) and (19), up to trivial factors, can now be recovered by substituting the second identity of Eq. (D5) into the above two equations, respectively. Q.E.D.

[1] *Femtosecond Chemistry*, edited by J. Manz and L. Wöste (VCH, Weinheim, 1995).
[2] *Ultrafast Processes in Chemistry and Photobiology*, edited by M. A. El-Sayed, I. Tanaka, and Y. Molin (Blackwell Science, Oxford, 1995).
[3] Y. J. Yan and S. Mukamel, J. Chem. Phys. **89**, 5160 (1988).
[4] S. Mukamel, *The Principles of Nonlinear Optical Spectroscopy* (Oxford University Press, New York, 1995).
[5] R. Kubo, Adv. Chem. Phys. **15**, 101 (1969).
[6] J. L. Martin and M. H. Vos, Annu. Rev. Biophys. Biomol. Struct. **21**, 199 (1992).
[7] M. H. Vos, M. R. Jones, C. N. Hunter *et al.*, Biochemistry **33**, 6765 (1994).
[8] Q. Wang, R. W. Schoenlein, L. A. Peteanu *et al.*, Science **266**, 422 (1994).
[9] K. Wynne, G. D. Reid, and R. M. Hochstrasser, J. Chem. Phys. **105**, 2287 (1996).
[10] D. C. Arnett, P. Vöhringer, and N. F. Scherer, J. Am. Chem. Soc. **117**, 12262 (1995).
[11] Y. Tanimura and S. Mukamel, J. Chem. Phys. **99**, 9496 (1993).
[12] V. Chernyak, W. M. Zhang, and S. Mukamel, J. Chem. Phys. **109**, 9587 (1998).
[13] K. Tominaga and K. Yoshihara, Phys. Rev. Lett. **74**, 3061 (1995).
[14] K. Tominaga and K. Yoshihara, Phys. Rev. Lett. **76**, 987 (1996).
[15] K. Tominaga and K. Yoshihara, Phys. Rev. A **55**, 831 (1997).
[16] T. Steffen and K. Duppen, Phys. Rev. Lett. **76**, 1224 (1996).
[17] A. Tokmakoff and G. R. Fleming, J. Chem. Phys. **106**, 2569 (1997).
[18] A. Tokmakoff, M. J. Lang, D. S. Larsen *et al.*, Phys. Rev. Lett. **79**, 2702 (1997).
[19] W. Zhao and J. C. Wright, Phys. Rev. Lett. **84**, 1411 (2000).
[20] S. Hahn, K. Kwak, and M. Cho, J. Chem. Phys. **112**, 4553 (2000).
[21] P. Hamm, M. Lim, W. F. DeGrado, and R. M. Hochstrasser, J. Chem. Phys. **112**, 1907 (2000).
[22] U. Weiss, *Quantum Dissipative Systems*, Series in Modern Condensed Matter Physics, 2nd ed. (World Scientific, Singapore, 1999), Vol. 10.
[23] F. Bloch, Phys. Rev. **105**, 1206 (1957).
[24] A. G. Redfield, Adv. Magn. Reson. **1**, 1 (1965).
[25] W. T. Pollard, A. K. Felts, and R. A. Friesner, Adv. Chem. Phys. **93**, 77 (1996).
[26] D. Kohen, C. C. Marson, and D. J. Tannor, J. Chem. Phys. **107**, 5236 (1997).
[27] Y. J. Yan, F. Shuang, R. X. Xu *et al.*, J. Chem. Phys. **113**, 2068 (2000).
[28] H. Dekker, Phys. Rep. **80**, 1 (1981).
[29] A. O. Caldeira and A. J. Leggett, Physica A **121A**, 587 (1983).
[30] G. Lindblad, Commun. Math. Phys. **48**, 119 (1976).
[31] V. Gorini, A. Kossakowski, and E. C. G. Sudarshan, J. Math. Phys. **17**, 821 (1976).
[32] R. Alicki and K. Lendi, *Quantum Dynamical Semigroups and Applications: Lecture Notes in Physics 286* (Springer, New York, 1987).
[33] Y. Tanimura and P. G. Wolynes, Phys. Rev. A **43**, 4131 (1991).
[34] Y. Tanimura and S. Mukamel, J. Chem. Phys. **101**, 3049 (1994).
[35] Y. Tanimura and Y. Maruyama, J. Chem. Phys. **107**, 1779 (1997).
[36] Y. J. Yan, Phys. Rev. A **58**, 2721 (1998).
[37] C. Meier and D. J. Tannor, J. Chem. Phys. **111**, 3365 (1999).
[38] J. L. Krause, M. Messina, K. R. Wilson, and Y. J. Yan, J. Phys. Chem. **99**, 13736 (1995).
[39] Z. W. Shen, Y. J. Yan, J. X. Cheng *et al.*, J. Chem. Phys. **110**, 7192 (1999).
[40] V. M. B. Fain and Y. I. Khanin, *Quantum Electronics* (Pergamon, New York, 1969).
[41] Y. J. Yan and S. Mukamel, Phys. Rev. A **41**, 6485 (1990).
[42] P. Cong, Y. J. Yan, H. P. Deuel, and J. D. Simon, J. Chem. Phys. **100**, 7855 (1994).
[43] C. Yang, F. Shuang, and Y. J. Yan, J. Chin. Chem. Soc. (Taipei) **47**, 799 (2000), Special issue: Ultrafast Phenomena in Spectroscopy.
[44] R. Loudon, *The Quantum Theory of Light*, 2nd ed. (Clarendon, Oxford, 1983).
[45] I. A. Walmsley, T. J. Dunn, J. Sweetser, and C. Radzewicz, in *Ultrafast Phenomena VIII*, edited by J.-L. Martin, A. Migus, G. A. Mourou, and A. H. Zewail (Springer-Verlag, Berlin, 1993), pp. 78–80.
[46] V. Wong and I. A. Walmsley, J. Opt. Soc. Am. B **12**, 1491 (1995).
[47] S. Mukamel, C. Ciordas-Ciurdariu, and V. Khidekel, Adv. Chem. Phys. **101**, 345 (1997).
[48] L. W. Ungar and J. A. Cina, Adv. Chem. Phys. **100**, 171 (1997).
[49] Y. J. Yan and S. Mukamel, J. Chem. Phys. **86**, 6085 (1987).
[50] J. C. Light, I. P. Hamilton, and J. V. Lill, J. Chem. Phys. **82**, 1400 (1985).
[51] W. E. Arnoldi, Q. Appl. Math. **9**, 17 (1951).
[52] T. J. Park and J. C. Light, J. Chem. Phys. **85**, 5870 (1986).
[53] E. Merzbacher, *Quantum Mechanics*, 3rd ed. (Wiley, New York, 1998).